

On the possibility of measuring the gluon distribution in proton with $\gamma + \text{jet}$ events at LHC

D.V. Bandurin¹ and N.B. Skachkov^{1a}

Joint Institute for Nuclear Research, Dubna, Russia

Received: / Revised version:

Abstract. The numbers of the $\gamma + \text{jet}$ events suitable for a determination of the gluon distribution function $f_g^p(x; Q^2)$ in a proton at the LHC for various intervals of x and Q^2 are estimated. The contributions of different background sources are studied. The values of discrimination powers between quark and gluon jets as well as between a single photon and the products of π^0 ; η and K_s^0 mesons decaying through the neutral channels are applied to estimate the final contributions of different event types to the $\gamma + \text{jet}$ production in various intervals of x and Q^2 . The PYTHIA event generator was used to produce physical events for this analysis.

PACS. 14.70.Dj Gluons { 14.20.Dh Protons and neutrons { 13.85.+t Hadron-induced high- and super-high-energy interactions.

^a Present address: Joliot-Curie 6, JINR, 141980, Dubna,

1 Introduction.

The modeling of the production processes of many new particles (Higgs boson, SUSY particles) in the forthcoming LHC experiments as well as future physical analysis of corresponding measurement are heavily based on the knowledge of gluon distribution in a proton $f_g^p(x; Q^2)$ [1]¹. For this reason the study of the possibility of the measuring gluon density directly in the LHC experiments (especially in the kinematic region of small x and high Q^2) is of a big interest.

One of the promising channels for this measurement is an inclusive prompt photon production [2]

$$pp \rightarrow \gamma^{dir} + X \quad (1)$$

The region of photon transverse momentum P_t , reached by UA1 [3], UA2 [4], CDF [5] and D0 [6] experiments, extends up to $P_t = 60 \text{ GeV} = c$ and, according to recent results [7], up to $P_t = 105 \text{ GeV} = c$. These data together with the later ones (see references in [8] [19]) and E706 [20], UA6 [21] results give, in principle, an opportunity for tuning the form of gluon distribution (see [13,16,22,23]). The rates and an estimation for cross sections of inclusive photon production at LHC are given in [2] (see also [24]).

Here we consider the process of a direct photon production in association with an opposite-side jet [12,13] (for experimental results see [25,26,27])

$$pp \rightarrow \gamma^{dir} + jet + X \quad (2)$$

In QCD leading order the processes (1) and (2) are caused by two subprocesses²: the "Compton-like" scattering

$$qg \rightarrow q + \gamma \quad (3)$$

and the "annihilation" subprocess

$$q\bar{q} \rightarrow g + \gamma \quad (4)$$

The first one gives a dominant contribution to the cross sections of (1) and (2) [8,12,13] and serves as "signal" subprocess due to its direct connection with the gluon distribution.

The study of " $\gamma + jet$ " process (2) is a more preferable as compared with the inclusive direct photon production process (1) from the viewpoint of extraction of information on the gluon distribution $f_g^p(x; Q^2)$ ³. First of all, it is explained by a higher value of a purity of the process (2), for which the signal-to-background ($S=B$) ratios are several times higher than $S=B$ ratios to process (1) [31,32]. Secondly, while the cross section for the process (1) is given as an integral over the parton distribution functions (PDF) of a proton $f_a^p(x; Q^2)$, the cross section of the process (2) is expressed directly (at $P_t = 30 \text{ GeV} = c$ ⁴) through these PDFs:

$$\frac{d}{d_1 d_2 d(P_t)^2} = \sum_{a,b} x_a f_a^p(x_a; Q^2) x_b f_b^p(x_b; Q^2) \frac{d}{df} (ab \rightarrow \gamma) \quad (5)$$

¹ For example, the production of Standard Model Higgs boson is mainly caused by gluon-gluon fusion $gg \rightarrow H$ over the entire mass range [1].

² A contribution of another possible NLO channel $gg \rightarrow g + \gamma$ was found to be still negligible even at LHC energies.

³ A detailed study of " $\gamma + jet$ " events and different aspects of their application can be found in [28,29].

⁴ i.e. in the region where " k_T smearing effects" should not be important (for example, see [18]).

where $a; b = q; \bar{q}; g; 1; 2 = q; \bar{q}; g$. The incident parton momentum fractions $x_a; x_b$ may be reconstructed from the final state photon and jet pseudorapidities $\eta_1 = \eta_{\text{jet}}$, $\eta_2 = \eta_{\text{jet}}$ and P_t according to formula⁵

$$x_{a,b} = \frac{P_t}{\sqrt{s}} (\exp(\eta_1) + \exp(\eta_2)) \quad (6)$$

Thus, formula (5) with the knowledge of the experimentally determined triple cross section in the intervals of η_{jet} and $(P_t)^2$ and with account of results of independent measurements of $q; \bar{q}$ distributions [33] allows the gluon distribution $f_g^p(x; Q^2)$ to be determined after essential reduction of a background contribution.

The P_t distributions of the number of signal events remained after application of strict selection criteria, proposed in [31,34], were presented earlier in [29,30,35,36]⁶. Those selection criteria allow to reduce considerably the background to $\gamma_{\text{dir}} + \text{jet}$ process (2) and select the events with a suppressed initial state radiation. Here we present the detailed study of background fraction in different x - and Q^2 -intervals and show that "gluonic" subprocess (3) gives a noticeable contribution [30].

This paper is organized as follows. The main background sources are discussed in section 2. In section 3 we list the selection criteria used to enhance the content of the signal events (3) in the selected data sample. In section 4 the numbers of the events suitable for an extraction of the gluon distribution function $f_g^p(x; Q^2)$ are estimated. The contribution of events of other types in different x - and Q^2 -intervals are also shown in this section. A possibility of the further background events suppression by an account of the discrimination efficiencies between a single photon and $\gamma; \eta; \omega$ and K_s^0 mesons as well as between quark and gluon jets is also demonstrated.

2 Background sources.

The background to the events based on the process (2) is mainly caused by:

- | the events with high P_t photons produced in the neutral decay channels of $\gamma; \eta; \omega$ and K_s^0 mesons⁷.
- | the events with the photons radiated from a quark (i.e. bremsstrahlung photons) in the next-to-leading order QCD subprocesses of the $q\bar{q} \rightarrow q\bar{q}\gamma, q\bar{q} \rightarrow q\bar{q}\gamma, q\bar{q} \rightarrow q\bar{q}\gamma$ and $q\bar{q} \rightarrow q\bar{q}\gamma$ scattering [31,32].

The background events of the first type will be called below as the "meson" events while the events of the second type as the "brems" ones. A more detailed information about fundamental QCD subprocesses from which originate "meson" and "brems" events is presented in section 3.

The background may be also caused by "e" events" which contain one jet and e as a direct photon candidate. The value of the fraction of these events in the total background was estimated in [31,32] (see also sections 3, 4).

The background containing the "meson" events can be significantly suppressed by the event selection criteria, pointed in [31,32,34]. It may be achieved, first of all, due to very strict photon isolation criteria because a parent

⁵ see, for instance, [11,12].

⁶ Analogous estimations for the Tevatron were done in [37,38].

⁷ As it was shown in [39] the charged decay channels of those mesons can be strongly suppressed even without a tracker information.

meson (π^0 ; η or K_s^0) is usually surrounded by other particles. Additional rejection factors were obtained from a full GEANT simulation of the physical processes in the CMS detector [40] where for the Barrel region ($|j| < 1.4$) we used an information from the electromagnetic calorimeter (ECAL) cells only⁸ [42] while for the Endcap region ($1.4 < |j| < 2.5$) the results of the analysis of hits in the preshower detector [43] were applied.

An especial attention should be paid to the events containing the bremsstrahlung photons. They are also noticeably rejected by the selection cuts but still constitute a significant part of the total background [31,32].

The simulation, performed with a help of the Monte Carlo event generator PYTHIA [44], has shown that in the selected " $\pi^0 + jet$ " event samples the most part of " $\pi^0 + brems$ " events contain a gluon jet (see section 4). For this part of events, as well as for a part of " $\pi^0 + mes$ " events with a gluon jet, one can take into consideration the quark/gluon separation efficiencies found earlier in [45]⁹. The number of remained background events also must be well estimated in order to separate their contribution from one of the " $\pi^0 + jet$ " events (2).

3 Definition of selection cuts¹⁰.

1. Only the events with one jet and one " π^0 -candidate" (in what follows we shall denote it also as π^0 and call the " π^0 " for brevity) with

$$P_t^{jet} > 30 \text{ GeV}/c \text{ and } P_t^{\pi^0} > 40 \text{ GeV}/c : \tag{7}$$

are considered here. In the simulation the signal (most energetic π^0 or e together with surrounding particles) is considered as a candidate for a direct photon if it fits into one CMS calorimeter tower having the size of 0.087×0.087 in the η space [40].

For all applications a jet is defined according to the PYTHIA jet finding algorithm LUCY [44]. In the η space the jet cone of radius R counted from the jet initiator cell is taken to be $R = (\Delta\eta^2 + \Delta\phi^2)^{1/2} = 0.7$.

2. To suppress the contribution of background processes, i.e. to select mostly the events with the " π^0 -isolated" photons and to discard the events that fake a direct photon signal, we restrict:

a) the value of the scalar sum of P_t of hadrons and other particles surrounding a photon within a cone of $R_{isol} = (\Delta\eta^2 + \Delta\phi^2)^{1/2} = 0.7$ (" π^0 -absolute isolation cut")

$$\sum_{i \in R_{isol}} P_t^i \leq P_t^{\pi^0} + P_{t_{CUT}}^{isol} ; \tag{8}$$

b) the value of a fraction (" π^0 -fractional isolation cut")

$$\sum_{i \in R_{isol}} P_t^i \leq P_t^{\pi^0} \cdot C_{CUT} ; \tag{9}$$

3. Only the events having no tracks¹¹ with $P_t > 1 \text{ GeV}/c$ contained inside the cone of $R = 0.4$ around a " π^0 -candidate" are accepted.

⁸ A preshower detector is not foreseen currently in the Barrel region of the CMS detector [40].

⁹ see also [46,47].

¹⁰ In this section we follow mostly the selection criteria from [31,34].

¹¹ i.e. charged particles as we use the PYTHIA level of simulation.

4. To suppress the background events with photons resulting from π^0 , η , ω and K_S^0 meson decays, we require the absence of a high P_t hadron in the tower containing the dir -candidate:

$$P_t^{\text{hadr}} < 7 \text{ GeV} = c; \quad (10)$$

At the PYTHIA level of simulation this cut may effectively take into account the imposing of an upper cut on the energy deposited in the cells of hadronic calorimeter (HCAL) that are behind the ECAL signal cells fired by the photon. In real experimental conditions one can require for a fraction of the photon energy, deposited in ECAL to be greater than some threshold¹².

5. We select the events with the vector P_t^{jet} being "back-to-back" to the vector P_t^{\sim} (in the plane transverse to the beam line) within the azimuthal angle interval defined by the equation:

$$(\phi_{\text{jet}}) = 180 \pm \Delta\phi; \quad (11)$$

The angle (ϕ_{jet}) between P_t^{\sim} and P_t^{jet} vectors is calculated from the expression $P_t^{\sim} P_t^{\text{jet}} = P_t^{\sim} P_t^{\text{jet}} \cos(\phi_{\text{jet}})$ with $P_t^{\sim} = \sqrt{P_t^2 - j^2}$ and $P_t^{\text{jet}} = \sqrt{P_t^2 - j^2}$. The value of $\Delta\phi$ may be chosen from the interval $5 \leq \Delta\phi \leq 15$ for various energies.

6. We also choose only the events that do not have any other, except one jet, m_{injet} (or cluster) high P_t activity with the P_t^{clust} higher than some threshold $P_{t_{\text{CUT}}}^{\text{clust}}$ value. Thus, we select events with

$$P_t^{\text{clust}} < P_{t_{\text{CUT}}}^{\text{clust}}; \quad (12)$$

where clusters are found by the same jet finder LUCCELL used to determine the main jet in the event. The most effective restrictions are $P_{t_{\text{CUT}}}^{\text{clust}} = 5 \leq 15 \text{ GeV} = c$. Their choice will be caused mostly by the gained statistics and P_t^{\sim} value (for higher P_t^{\sim} a weaker $P_{t_{\text{CUT}}}^{\text{clust}}$ can be used).

7. The events containing e as a photon candidate are mainly caused by the subprocesses $q\bar{q} \rightarrow q^0 + W$ and $q\bar{q} \rightarrow g + W$ with the subsequent decay $W \rightarrow e$. To reduce a contribution from these events [1,32] we shall select only events having a small value of missing transverse momentum P_t^{miss} . So, we also use the following cut:

$$P_t^{\text{miss}} < P_{t_{\text{CUT}}}^{\text{miss}}; \quad (13)$$

Finally, in what follows we shall set the values of the cut parameters (besides those pointed above explicitly) as specified below:

$$P_{t_{\text{CUT}}}^{\text{isol}} = 2 \text{ GeV} = c; \quad P_{t_{\text{CUT}}}^{\text{clust}} = 5\%; \quad \Delta\phi = 15; \quad (14)$$

$$P_{t_{\text{CUT}}}^{\text{clust}} = 10 \text{ GeV} = c; \quad P_{t_{\text{CUT}}}^{\text{miss}} = 10 \text{ GeV} = c; \quad (14)$$

¹² e.g. to be greater than 0.95 (as it was used at D0 [7])

4 Determining the numbers of events and reducing the background.

To estimate a background to the signal events we have done a simulation using the Monte Carlo event generator PYTHIA with a mixture of all existing in PYTHIA QCD and SM subprocesses with large cross sections¹³, including subprocesses (3) and (4)¹⁴.

The total cross section of the background subprocesses exceeds the cross section of the subprocesses (3) and (4) by more than three orders of magnitude. The GRV94L parameterization of the parton distribution functions is used as a default one.

Five generations (each of about 60{90 million events) with different values of minimal transverse momentum of a hard subprocess¹⁵ p_{\perp}^m were done: $p_{\perp}^m = 40, 70, 100, 140$ and 200 GeV=c. The cross sections of the above mentioned subprocesses define the rates of corresponding physical events and, thus, appear here as weight factors. The selection criteria of section 3 were applied then to the generated events.

The total numbers of these events, i.e. events originated from subprocesses (3) and (4) as well as "bremsstrahlung" and "meson" events, are presented (being divided by the factor of 10^3) in Table 1 for each x and Q^2 interval ($Q^2 = (P_t^e)^2$) for the integrated luminosity¹⁶ $L_{int} = 10 \text{ fb}^{-1}$. The momentum fractions x_a and x_b of the initial state partons were calculated via the photon and jet parameters according to formula (6) [11,12]. The right-hand columns of this table shows, for a convenience, the correspondence of Q^2 interval to the P_t^e interval.

One can see from Table 1 that at $40 < P_t^e < 50$ GeV=c the total number of events is about 10 million and it drops to 24 200 at $200 < P_t^e < 283$ GeV=c, i.e. with five-fold increase of P_t^e the spectrum drops about 400 times.

The contribution from the background "e events" was not included in Table 1. The number of these type events was estimated in [31,32]¹⁷ and found to be very small as compared with other background types. Thus, in what follows we shall concentrate on more sizable background.

Now let us look at the contributions of different event types in various x and Q^2 intervals. The events selected after passing the criteria of section 3 were classified in accordance with the origin of the produced dir -candidates. So, we consider separately those that contain the direct photons (produced in subprocesses (3) and (4)) and those that have dir -candidates appearing due to the radiation from quarks ("bremsstrahlung" events) or from the $0, \gamma, \mu$ and K_S^0 meson decays ("meson" events). All these contributions are presented in Tables 1A {4A of Appendix in a form of number of events divided by the factor of 10^3 . The numbers of the events based on the Compton (3) and annihilation (4) subprocesses are shown in Tables 1A and 2A while the numbers of the "bremsstrahlung" and "meson" events can be

¹³ They have ISUB= 11{20, 28{31, 53, 68 according to the process numbers in PYTHIA [44].

¹⁴ with ISUB= 14 and 29 in notations of PYTHIA [44].

¹⁵ CKIN (3) parameter in PYTHIA.

¹⁶ This value is intended to be accumulated during one year of LHC running at luminosity $L = 10^{33} \text{ cm}^{-2} \text{ s}^{-1}$.

¹⁷ It was found that after application of the selection criteria from section 3 and taking a tracking efficiency to be equal to 85% (being averaged over all pseudorapidity range) [41] a contribution of the e events (having the isolated e with $P_t^e > 40$ GeV=c) to the total background reduces to less than 1% at $P_t^e = 70$ GeV=c and to about 5% at $P_t^e = 100$ GeV=c.

found in Tables 3A and 4A, respectively¹⁸. These numbers were obtained after passing the selection criteria of section 3. The fractions of each event type, calculated for a given interval of $P_{t\sim}$, are presented in Fig. 1a (100% is taken for all types of events).

We see that the main part of the background is due to γ brem events and the combined contribution of γ brem and γ mes events into the total number of events varies from about 23% at $40 < P_{t\sim} < 50$ GeV=c to about 6% at $100 < P_{t\sim} < 140$ GeV=c and drops to 4% at $200 < P_{t\sim} < 283$ GeV=c.

We would like to stress that the essential point of our analysis is the study of the background contributions after application of the cuts for selecting the $\gamma + \text{jet}$ events with a limited cluster/minijet activity and a clean jet topology¹⁹. Only in this case a contribution of γ brem and γ mes events can be decreased noticeably²⁰.

The selection criteria of section 3 are not final and are moderate enough. The results of their application may change if we shall vary some cuts. So, for example, a stronger limitation of cluster activity (12) by $P_{tCUT}^{chist} = 5$ GeV=c would lead to a further substantial decreasing of the numbers of γ brem and γ mes events [31,32].

The contribution of γ mes events can be also reduced by the account of the difference between a single photon and the π^0 , η , ω and K_s^0 meson signals produced in the detector.

To take into account the discrimination efficiencies between a single photon and the photons produced via multi-photon decays of π^0 , η , ω and K_s^0 mesons (π^0 mes), the results of papers [42] and [43] were used. The efficiencies found in [42] were obtained by the analysis of the ECAL crystal cells only in the Barrel region ($|j| < 1.4$) while the efficiencies in [43] are found from the analysis of hits in the preshower detector in the Endcap region ($1.4 < |j| < 2.5$). The results of [42] and [43] are briefly the following: the rejection efficiency of the neutral pion is about 49–67% (depending on an energy) in the Barrel region and it ranges as 45–71% for the Endcap region. The single photon selection efficiencies (ϵ_{sel}) were set to 70% and 91% in the first and second cases respectively²¹.

The results of applications of the described above meson separation efficiencies to the γ mes events themselves are placed in Table 8A (compare with Table 4A) and in Tables 5A–7A of Appendix for other event types. Thus, we see that for the γ mes events the reduction factor of about 2–3 for $40 < P_{t\sim} < 100$ GeV=c can be obtained with

¹⁸ See also [31,32] for a more detailed information about background composition.

¹⁹ See [31,32] where the dynamics of application of the selection criteria is demonstrated.

²⁰ It was shown in [31,32] that, for instance, at $P_{t\sim} > 100$ GeV=c, the application of "photonic" cuts, usually used to select inclusive photon $\gamma + X$ events, gives $S=B = 1:9$ only, while a further account of "hadronic" and topological cuts for selection of $\gamma + \text{jet}$ events leads to $S=B = 17:6$, i.e. to the increase of $S=B$ by about one order of magnitude (here S is a total contribution from the events based on the subprocesses (3) and (4) and B is a contribution from the sum of γ brem and γ mes events). The application of other cuts that limit a $P_{t\sim}$ activity out of the $\gamma + \text{jet}$ system may lead to the following 20–30% increase of the $S=B$ ratio [31,32].

²¹ With the same $\epsilon_{sel} = 70\%$ one can also reject about 90–95% of γ meson events and 55–92% of K_s^0 meson events [42] in the Barrel region. For the Endcap the respective rejection efficiencies were taken here equal to those obtained for π^0 meson. At the same time it is worth to note that the main contribution to the γ mes background comes from the π^0 -events (62–65% in the interval $40 < P_{t\sim} < 140$ GeV=c) [31,32].

a loss of 16–19% of events of other types with a single photon in the final state. The total numbers of all events left after account of the m_{es} separation efficiencies are presented in Table 2.

The physical models implemented in PYTHIA allow us to get an idea about a possible origination of the $\backslash \text{brem}''$ and $\backslash \text{mes}''$ events. Tables 3 and 4 show the relative contributions of four main (having the largest cross sections) fundamental QCD subprocesses $q\bar{q} \rightarrow q\bar{q}, q\bar{q} \rightarrow q\bar{q}, g\bar{g} \rightarrow q\bar{q}$ and $g\bar{g} \rightarrow g\bar{g}$ into a production of the $\backslash \text{brem}''$ and $\backslash \text{mes}''$ events selected with the criteria 1{7 of section 3 for three $P_{t^{\sim}}$ intervals²². One can see from these tables that most of $\backslash \text{brem}''$ and $\backslash \text{mes}''$ events (from 70 to 80%) still originate from $\backslash \text{gluonic}''$ $q\bar{q} \rightarrow q\bar{q}, g\bar{g} \rightarrow q\bar{q}$ and $g\bar{g} \rightarrow g\bar{g}$ subprocesses with dominant contribution from the first subprocess.

The analysis of the PYTHIA simulation output also shows that practically in all of selected $\backslash \text{brem}''$ events the $\backslash \text{brem strahlung photons}''$ are produced in the final state of the fundamental subprocess. They are radiated from the outgoing quarks in the case of the first three subprocesses or can appear as the result of string breaking in the case of $g\bar{g} \rightarrow g\bar{g}$ scattering. The last mechanism, naturally, gives a small contribution into the $\backslash \text{brem}''$ events production. In the first case the selected (see section 3) photon carries away almost all energy of a quark in the final state. The events of this kind have mostly a gluon jet (70:6% of events for $40 < P_{t^{\sim}} < 71 \text{ GeV} = c$ interval and 58:7% of events for $141 < P_{t^{\sim}} < 283 \text{ GeV} = c$) with the photon radiated in back-to-back direction to the jet in the plane. In the second case ($g\bar{g} \rightarrow g\bar{g}$ based events) a remained jet is practically always of the gluon type.

As for $\backslash \text{mes}''$ events, it is naturally to expect that in the events based on the $q\bar{q} \rightarrow q\bar{q}$ scattering after suppression of the cluster activity by the cut $P_{t^{\text{clust}}} < 10 \text{ GeV} = c$ (see (12)) a remained jet can originate with an equal probability from a quark as well as from a gluon (50% by 50%) while in the events based on the $q\bar{q} \rightarrow q\bar{q}, g\bar{g} \rightarrow q\bar{q}$ ($g\bar{g} \rightarrow g\bar{g}$) subprocesses the jet is always of the quark (gluon) type.

Thus, one can conclude that about 73% (40%), 70% (36%) and 59% (33%) of the $\backslash \text{brem}''$ ($\backslash \text{mes}''$) events have a gluon jet in the selected one-jet events in $P_{t^{\sim}}$ intervals $40-71, 71-141$ and $141-283 \text{ GeV} = c$, respectively.

For the following suppression of the contributions from $\backslash \text{brem}''$ and $\backslash \text{mes}''$ events having a gluon jet in the final state one can apply the quark/gluon separation efficiencies ($\epsilon^{q=g}$) obtained earlier in [45]. The results of [45] shows that with account of the quark jet selection efficiency of about 65–67% it is possible to reject 73–81% of gluons jets²³ for $P_{t^{\text{jet}}}$ varying from 40 to 200 $\text{GeV} = c$.

The numbers of different types of events after an account of the both m_{es} and $\epsilon^{q=g}$ separation efficiencies are presented in Tables 9A (12A of Appendix while their fractions (in %) are shown in Fig. 1c.

By comparing Tables 7A and 11A one can see that the numbers of $\backslash \text{brem}''$ events²⁴ are reduced in 2:5–3 times at the cost of 35% loss of the events based on subprocess (3) and their fraction in the total number of events

²² The sum over contributions from the four considered QCD subprocesses in some lines of Tables 3 and 4 is less than 100%. The remained percentages correspond to other subprocesses (like $q\bar{q} \rightarrow q\bar{q}$ or $q\bar{q} \rightarrow q^0W$). The errors in those tables are statistical and caused by the number of entries for various background types after application of the criteria 1{7 of section 3.

²³ This efficiency slightly depends on the jet transverse momentum $P_{t^{\text{jet}}}$ and pseudorapidity η^{jet} [45].

²⁴ that are, in fact, irreducible by using only photon information after application of the strong isolation cuts (8) and (9).

becomes about 8% at $40 < P_{t\sim} < 50 \text{ GeV} = c$ and about 2% at $140 < P_{t\sim} < 200 \text{ GeV} = c$. The total contributions of the $\backslash \text{ brem} \text{''}$ and $\backslash \text{ mes} \text{''}$ events in the same $P_{t\sim}$ intervals compose 13.2% and 2.8%, respectively.

We see also that the account of $q=g$ separation efficiency reduces a contribution of the events originated from annihilation subprocess (4) to the total number of events (especially at higher $P_{t\sim}$) to the size of about 3–5% over all considered $P_{t\sim}$ range (see Fig. 1 and Tables 1A–1A).

The final numbers of all $\backslash + \text{ jet} \text{''}$ events for the luminosity $L_{\text{int}} = 10 \text{ fb}^{-1}$ at different x and Q^2 intervals after an account of the both separation efficiencies are given in Table 5. We see that after passing all selection cuts and application of the $q=g$ and $q=g$ efficiencies one can get about 5 million events at the $40 < P_{t\sim} < 50 \text{ GeV} = c$ interval, about 200 000 at $100 < P_{t\sim} < 141 \text{ GeV} = c$ and about 11 000 at the last considered interval $200 < P_{t\sim} < 283 \text{ GeV} = c$. The total expected statistics on the $\backslash + \text{ jet} \text{''}$ events, left after account of the $q=g$ and $q=g$ efficiencies, is about $9 \cdot 10^6$ events. The final contributions of different subprocesses in various x and Q^2 intervals are presented in Tables 9A–12A.

5 Conclusion.

The results presented above show that during one year of the LHC running at low luminosity ($L = 10^{33} \text{ cm}^{-2} \text{ s}^{-1}$) one can collect after application of the proposed selection criteria the clean sample of $\backslash^{\text{dir}} + \text{ jet} \text{''}$ events with a sufficient statistics to determine a gluon density in a proton in new kinematic region of $2 \cdot 10^{-4} < x < 1$ and $1.6 \cdot 10^2 < Q^2 < 2 \cdot 10^5 \text{ (GeV} = c)^2$. At the same time the combined contribution of $\backslash \text{ brem} \text{''}$ events and $\backslash \text{ mes} \text{''}$ events is estimated to be about 23% at $40 < P_{t\sim} < 50 \text{ GeV} = c$ and it drops to 4% at $200 < P_{t\sim} < 283 \text{ GeV} = c$ (see Tables 1A–4A and Fig. 1a).

The given estimations on contributions of the $\backslash \text{ brem} \text{''}$ and $\backslash \text{ mes} \text{''}$ events are not final yet. For instance, a stronger limitation $P_{t\text{cut}}^{\text{chist}} = 5 \text{ GeV} = c$ (see (12)) would lead to a following substantial (about 30%) reduction of their contribution [31,32].

With an additional account of discrimination efficiencies between single photons and $0; K_s^0$ mesons as well as those between quark and gluon jets [42,43,45] one can increase noticeably the purity of the selected samples of the $\backslash^{\text{dir}} + \text{ jet} \text{''}$ events (see Tables 9A–12A of Appendix and Fig. 1). A possibility to obtain better background rejection factors will depend on the chosen values of single photon and quark jet selection efficiencies²⁵ which are in their turn will be caused by a gained statistics of the $\backslash + \text{ jet} \text{''}$ events.

It is also worth mentioning that a full simulation²⁶ of the signal and background processes is rather difficult due to a very small selection efficiency for the background events (~ 0.01 – 0.05% depending on an energy) [31,32] what, in its turn, requires huge computational resources to collect the background events statistics sufficient for the analysis.

²⁵ Let us remind that the single photon selection efficiencies equal to 70% and 91% for the Barrel and Endcap regions and quark jet selection efficiencies equal to about 65% were chosen here for the given estimations.

²⁶ We mean a full simulation of the detector response with the following digitization and reconstruction of signals from physical objects.

Fig. 2 shows in the widely used $(x; Q^2)$ kinematic plot (see also [48]) what area can be covered for studying the process $qg \rightarrow q + \text{jet}$. From this figure (and Tables 1, 2, 5) it becomes clear that even at low LHC luminosity it would be possible to study the gluon distribution with a good statistics of $\gamma + \text{jet}$ events in the region of small x at values of Q^2 that are about 2 orders of magnitude higher than those reached at HERA now. It is worth emphasizing that an extension of experimentally reachable region at LHC to the region of lower values of Q^2 , overlapping with the area covered by HERA, would be also of a big interest.

Acknowledgments

We are greatly thankful to D. Denegri who stimulated us to study the physics of $\gamma + \text{jet}$ processes, permanent support and fruitful suggestions. It is a pleasure for us to express our recognition for helpful discussions to P. Aurenche, M. Dittmar, M. Fontannaz, J.Ph. Guillet, M.L. Mangano, E. Pilon, H. Rohringer, S. Tapprogge, H. Weerts and J. Womersley.

References

1. D. Denegri et al, "Summary of the CMS Discovery Potential for the MSSM SUSY Higgses", CMS NOTE 2001/032; S. Abdullin et al, "Discovery potential for supersymmetry in CMS", J.Phys.G 28 (2002)469, hep-ph/9806366; R. Kinnunen, "Higgs physics at LHC", CMS conference report, CMS CR 2002/020.
2. P. Aurenche et al. Proc. of "ECFA LHC Workshop", Aachen, Germany, 4-9 Octob. 1990, edited by G. Jarlskog and D. Rein (CERN-Report No 90-10; Geneva, Switzerland 1990), Vol. II.
3. UA1 Collaboration, C. Abajar et al, Phys.Lett. 209B (1988)385.
4. UA2 Collaboration, R. Ansari et al, Phys.Lett. 176B (1986)239.
5. CDF Collaboration. F. Abe et al, Phys.Rev.Lett. 68 (1992)2734; F. Abe et al, Phys.Rev.D 48 (1993)2998; F. Abe et al, Phys.Rev.Lett. 73 (1994)2662.
6. D0 Collaboration, F. Abachiet al, Phys.Rev.Lett. 77 (1996)5011.
7. D0 Collaboration, B. Abbott et al, Phys.Rev.Lett. 84 (2000)2786; D0 Collaboration, V. Abazov et al, Phys.Rev.Lett. 87 (2001)251805.
8. P. Aurenche, J. Lindfors, Nucl.Phys.B 168 (1980)296.
9. P. Aurenche, A. Douiri, R. Baier, M. Fontannaz, D. Schi, Phys.Lett.B 140 (1984)87.
10. T. Ferbel and W. R. Molzon, Rev.Mod.Phys. 56 (1984)181.
11. J.F. Owens, Rev.Mod.Phys. 59 (1987)465.
12. E.N. Argyres, A.P. Contogouris, N. Mebarki and S.D.P. Vassopoulos, Phys.Rev.D 35, (1987)1584.
13. P. Aurenche, et al Phys.Rev.D 39 (1989)3275.
14. E.L. Berger and J. Qiu, Phys.Rev.D 44 (1991)2002.
15. J. Huston et al, Phys.Rev.D 51 (1995)6139.
16. W. Vogelsang and A. Vogt, Nucl.Phys.B 453 (1995)334.

17. W. Vogelsang and M. Wally, *J Phys. G* 23 (1997)A1.
18. J. Huston ATLAS Note ATL-Phys-99-008, CERN, 1999.
19. S. Frixione and W. Vogelsang, CERN-TH/99-247 hep-ph/9908387.
20. E706 Collaboration, L. Apanasevich et al, *Phys Rev Lett.* 81 (1997)2642.
21. UA6 Collaboration, G. Balocchi et al, *Phys Lett. B* 436 (1998)222.
22. A.D. Martin et al, *Eur Phys J. C* 4 (1998)463.
23. CTEQ-C Collaboration, H.L. Lai et al, *Eur Phys J. C* 12 (2000)375.; see also <http://www.physpsu.edu/~cteq>.
24. P. Aurenche, M. Fontannaz, S. Frixione, *Proc. of CERN Workshop on Standard Model Physics (and more) at the LHC*, QCD (section 6.1) "General features of photon production", Yellow Report CERN-2000-004, 9 May 2000, CERN, Geneva.
25. ISR (AFSC) Collaboration, T. Akeesson et al, *Zeit Phys. C* 34 (1987)293.
26. UA2 Collaboration, J. Alitti et al, *Phys Lett. B* 299 (1993)174.
27. CDF Collaboration, F. Abe et al, *Phys Rev. D* 57 (1998)1359 (see also p.67).
28. D.V. Bandourin, V.F. Konoplyanikov, N.B. Skachkov, "On the application of $\gamma + \text{jet}$ events for setting the absolute jet energy scale and determining the gluon distribution at the LHC.", hep-ex/0207028.
29. D.V. Bandourin, V.F. Konoplyanikov, N.B. Skachkov, "Events rate estimation for gluon distribution determination at LHC", hep-ex/0207028. *Proc. of the XV ISHEP "Relativistic Nuclear Physics and Quantum Chromodynamics"*, Eds. A.M. Baldin, V.V. Burov, A.I. Malakhov. Dubna, 2001, v.I, pp.375-383.
30. D.V. Bandourin, N.B. Skachkov, "On the possibilities of measuring gluon distribution in $\gamma + Z0 + \text{jet}$ events at Tevatron Run II and LHC energies", Contributed to *Proc. of XI International Workshop on Deep Inelastic Scattering*, St. Petersburg, 2003.
31. D.V. Bandourin, V.F. Konoplyanikov, N.B. Skachkov, "Jet energy scale setting with $\gamma + \text{jet}$ events at LHC energies. Detailed study of the background suppression." JINR preprint E2-2000-255, hep-ex/0011017.
32. D.V. Bandourin, V.F. Konoplyanikov, N.B. Skachkov. "Setting the absolute scale for jet energy at CMS with $pp \rightarrow \text{jet} + X$ events. Study of background suppression (To appear as CMS Note).
33. M. Dittmar, F. Pauss, D. Zurcher, *Phys Rev. D* 56 (1997)7284.
34. D.V. Bandourin, V.F. Konoplyanikov, N.B. Skachkov, "Jet energy scale setting with $\gamma + \text{jet}$ events at LHC energies. Generalities, selection rules." JINR preprint E2-2000-251, hep-ex/0011012.
35. D.V. Bandourin, V.F. Konoplyanikov, N.B. Skachkov, " $\gamma + \text{jet}$ events rate estimation for gluon distribution determination at LHC", *Part Nucl Lett.* 103 (2000)34, hep-ex/0011015.
36. M. Dittmar, K. Mazumdar, N. Skachkov, *Proc. of CERN Workshop on Standard Model Physics (and more) at the LHC*, QCD (section 2.7), "Measuring parton luminosities and parton distribution functions", Yellow Report CERN-2000-004, 9 May 2000, CERN, Geneva.
37. D.V. Bandourin, N.B. Skachkov. " $\gamma + \text{jet}$ process application for setting the absolute scale of jet energy and determining the gluon distribution at the Tevatron Run II." D0 Note 3948, 2002, hep-ex/0203003.
38. D.V. Bandourin, N.B. Skachkov, "Photon+jet event rate estimation for gluon distribution determination at the Tevatron Run II", Contributed to *Proc. of XVI ISHEP "Relativistic Nuclear Physics and Quantum Chromodynamics"*, Dubna, 2002. JINR Preprint E2-2002-154, hep-ex/0206040, To appear in *Yad. Fiz.*

39. D.V. Bandourin, V.F. Konoplyanikov, N.B. Skachkov, "On the possibility of discrimination between π^0 ; η ; K_S^0 mesons and a photon based on the calorimeter information in the CMS detector", JINR Communication E1-2001-261, hep-ex/0108050.
40. CMS Electromagnetic Calorimeter Project, Technical Design Report, CERN/LHCC 97(33, CMS TDR 4, CERN, 1997.
41. CMS Tracker Project, Technical Design Report, CERN/LHCC 98(6, CMS TDR 5, CERN, 1999.
42. D.V. Bandourin, N.B. Skachkov. "Separation of a single photon and products of the π^0 ; η ; K_S^0 mesons neutral decay channels in the CMS electromagnetic calorimeter using neural network", JINR Communication E2-2001-259, hep-ex/0108051.
43. A. Kyriakis, D. Loukas, J. Mousa, D. Bamey, CMS Note 1998/088, "Artificial neuralnet approach to π^0 discrimination using CMS Endcap preshower".
44. T. Sjöstrand, Comp Phys Comm . 82 (1994)74. The version 6.131 of PYTHIA was used.
45. D.V. Bandourin, N.B. Skachkov, "Separation of quark and gluon jets in the direct photon production processes at the LHC using the neural network approach", JINR Communication E2-2001-260, hep-ex/0109001.
46. L. Lonnblad, C. Peterson and T. Rognvaldsson, "Finding gluon jets with a neural trigger", Phys Rev Lett, 65 (1990)1321.
47. L. Lonnblad, C. Peterson and T. Rognvaldsson, "Using neural network to identify jets", Nucl Phys., B 349 (1991)675.
48. R. Ball, M. Dittmar, W.J. Stirling, Proc. of "CERN Workshop on Standard Model Physics (and more) at the LHC", QCD, (section 2) "Parton distribution functions", Yellow Report CERN-2000-004, CERN, 2000.

List of figures

1. The contributions of various events types to the total number of events as a function of P_t presented for three cases: (a) No separation efficiency is taken into account, (b) $q=es$ separation efficiencies are taken into account and (c) $q=es$ and $q=g$ separation efficiencies are taken into account.
2. LHC ($x; Q^2$) kinematic region for $pp \rightarrow \gamma + \text{jet}$ process.

List of tables

1. Numbers of all events in different Q^2 and x intervals for $L_{int} = 10 \text{ fb}^{-1}$.
2. Numbers of all events in different Q^2 and x intervals for $L_{int} = 10 \text{ fb}^{-1}$. $q=es$ separation efficiencies are taken into account.
3. Relative contribution (in per cents) of different QCD subprocesses into the $\gamma + \text{jet}$ events production.
4. Relative contribution (in per cents) of different QCD subprocesses into the $q=es$ events production.
5. Numbers of all events in different Q^2 and x intervals for $L_{int} = 10 \text{ fb}^{-1}$. $q=es$ and $q=g$ separation efficiencies are taken into account.

Appendix

- 1A. Numbers of $\gamma + \text{jet}$ events in Q^2 and x intervals at $L_{int} = 10 \text{ fb}^{-1}$.
- 2A. Numbers of $\gamma + \text{jet}$ events in Q^2 and x intervals at $L_{int} = 10 \text{ fb}^{-1}$.
- 3A. Numbers of $\gamma + \text{jet}$ events in Q^2 and x intervals at $L_{int} = 10 \text{ fb}^{-1}$.
- 4A. Numbers of $q=es$ events in Q^2 and x intervals at $L_{int} = 10 \text{ fb}^{-1}$.
- 5A. Numbers of $\gamma + \text{jet}$ events in Q^2 and x intervals at $L_{int} = 10 \text{ fb}^{-1}$. $q=es$ separation efficiencies are taken into account.
- 6A. Numbers of $\gamma + \text{jet}$ events in Q^2 and x intervals at $L_{int} = 10 \text{ fb}^{-1}$. $q=es$ separation efficiencies are taken into account.
- 7A. Numbers of $\gamma + \text{jet}$ events in Q^2 and x intervals at $L_{int} = 10 \text{ fb}^{-1}$. $q=es$ separation efficiencies are taken into account.
- 8A. Numbers of $q=es$ events in Q^2 and x intervals at $L_{int} = 10 \text{ fb}^{-1}$. $q=es$ separation efficiencies are taken into account.
- 9A. Numbers of $\gamma + \text{jet}$ events in Q^2 and x intervals at $L_{int} = 10 \text{ fb}^{-1}$. $q=es$ and $q=g$ separation efficiencies are taken into account.
- 10A. Numbers of $\gamma + \text{jet}$ events in Q^2 and x intervals at $L_{int} = 10 \text{ fb}^{-1}$. $q=es$ and $q=g$ separation efficiencies are taken into account.
- 11A. Numbers of $\gamma + \text{jet}$ events in Q^2 and x intervals at $L_{int} = 10 \text{ fb}^{-1}$. $q=es$ and $q=g$ separation efficiencies are taken into account.
- 12A. Numbers of $q=es$ events in Q^2 and x intervals at $L_{int} = 10 \text{ fb}^{-1}$. $q=es$ and $q=g$ separation efficiencies are taken into account.

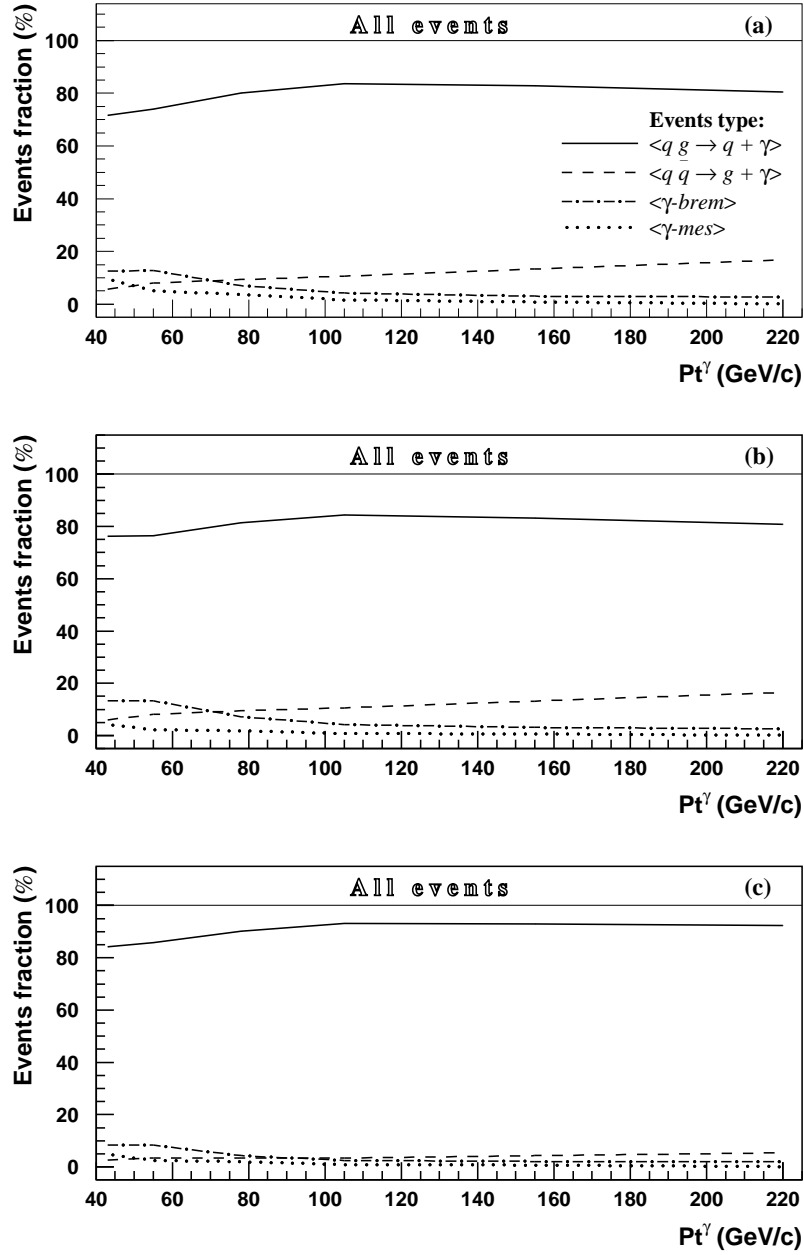


Fig. 1. The contributions of various events types to the total number of events as a function of P_t^γ presented for three cases: (a) No separation efficiency is taken into account, (b) $q=g$ separation efficiencies are taken into account and (c) $q=g$ separation efficiencies are taken into account.

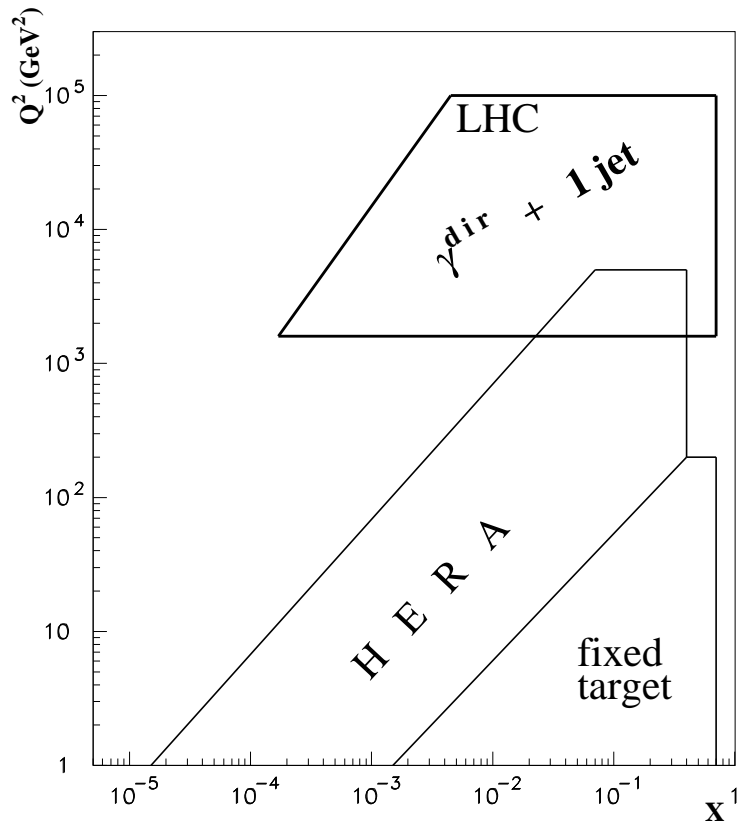


Fig. 2. LHC ($x; Q^2$) kinematic region for $pp \rightarrow \gamma + \text{jet}$ process.

Table 1. Numbers of all events (divided by 10^3) in Q^2 and x intervals for $L_{int} = 10 \text{ fb}^{-1}$.

Q^2 (GeV=c) ²	x values of a parton				All x $10^4\{10^0$	P_t (GeV=c)
	$10^4\{10^3$	$10^3\{10^2$	$10^2\{10^1$	$10^1\{10^0$		
1600-2500	1393.6	4301.1	4506.8	481.4	10682.9	40{50
2500-5000	561.1	2931.0	3174.7	430.4	7097.2	50{71
5000-10000	61.7	665.6	769.6	196.1	1693.0	71{100
10000-20000	3.6	150.3	178.4	81.7	414.0	100{141
20000-40000	0.0	29.9	40.9	25.2	96.0	141{200
40000-80000	0.0	5.7	10.7	7.8	24.2	200{283
					20 007.3	

Table 2. Numbers of all events (divided by 10^3) in Q^2 and x intervals for $L_{int} = 10 \text{ fb}^{-1}$. ϵ_{mes} separation efficiencies are taken into account.

Q^2 (GeV=c) ²	x values of a parton				All x $10^4\{10^0$	P_t (GeV=c)
	$10^4\{10^3$	$10^3\{10^2$	$10^2\{10^1$	$10^1\{10^0$		
1600-2500	1214.6	3073.1	3433.1	394.5	8115.4	40{50
2500-5000	502.8	2220.7	2478.2	364.0	5565.8	50{71
5000-10000	54.1	532.8	587.8	168.7	1343.7	71{100
10000-20000	3.2	124.4	134.6	70.6	333.1	100{141
20000-40000	0.0	25.3	30.1	21.8	77.3	141{200
40000-80000	0.0	4.9	7.9	6.6	19.4	200{283
					15 454.7	

Table 3. Relative contribution (in per cents) of main QCD subprocesses into the $\gamma\gamma$ events production.

P_t (GeV=c)	fundamental QCD subprocess							
	gg → gg		qq → qq		gg → qq		gg → gg	
40{71}	70.6	8.7	21.1	3.8	5.1	1.6	2.6	1.0
71{141}	67.5	7.3	23.6	3.5	4.2	1.2	2.6	0.9
141{283}	58.7	9.0	30.7	5.7	1.8	1.0		

Table 4. Relative contribution (in per cents) of main QCD subprocesses into the $\gamma e\gamma$ events production.

P_t (GeV=c)	fundamental QCD subprocess							
	gg → gg		qq → qq		gg → qq		gg → gg	
40{71}	65.2	9.9	20.1	4.5	7.1	2.5	7.2	2.3
71{141}	63.7	11.6	23.0	5.2	7.2	2.6	4.4	1.4
141{283}	57.7	26.2	23.1	13.9	7.7	6.9	3.8	4.6

Table 5. Numbers of all events (divided by 10^3) in Q^2 and x intervals for $L_{int} = 10 \text{ fb}^{-1}$. $\gamma\gamma$ and $\gamma e\gamma$ separation efficiencies are taken into account.

Q^2 (GeV=c) ²	x values of a parton				All x $10^{-4}\{10^0$	P_t (GeV=c)
	$10^{-4}\{10^{-3}$	$10^{-3}\{10^{-2}$	$10^{-2}\{10^{-1}$	$10^{-1}\{10^0$		
1600-2500	721.3	1858.7	2052.9	217.6	4850.5	40{50}
2500-5000	302.3	1314.1	1449.4	206.2	3271.9	50{71}
5000-10000	31.5	320.0	350.0	99.9	801.5	71{100}
10000-20000	1.9	74.4	81.1	41.8	199.1	100{141}
20000-40000	0.0	14.9	18.2	12.6	45.6	141{200}
40000-80000	0.0	2.9	4.5	3.8	11.2	200{283}
					9 179.8	

Appendix

Table 1A .Numbers of $q\bar{q} \rightarrow q + \bar{q}$ events (divided by 10^3) in Q^2 and x intervals at $L_{int} = 10 \text{ fb}^{-1}$.

Q^2 (GeV 2)	x values of a parton				All x 10^{-4}
	10^{-4}	10^{-3}	10^{-2}	10^{-1}	
1600-2500	1040.3	3128.7	3202.5	275.6	7647.1
2500-5000	451.2	2185.8	2326.8	280.8	5244.6
5000-10000	45.4	545.5	611.8	151.6	1354.4
10000-20000	2.9	125.5	151.1	66.7	346.2
20000-40000	0	24.6	35.2	19.9	79.6
40000-80000	0	4.7	8.5	6.2	19.4

Table 2A .Numbers of $q\bar{q} \rightarrow q + g$ events (divided by 10^3) in Q^2 and x intervals at $L_{int} = 10 \text{ fb}^{-1}$.

Q^2 (GeV 2)	x values of a parton				All x 10^{-4}
	10^{-4}	10^{-3}	10^{-2}	10^{-1}	
1600-2500	120.3	190.2	236.8	50.5	597.8
2500-5000	43.1	239.7	250.1	35.3	568.2
5000-10000	7.7	60.5	69.0	20.5	157.7
10000-20000	0.7	16.9	15.9	10.3	43.8
20000-40000	0	4.2	4.4	4.2	12.8
40000-80000	0	0.9	1.8	1.4	4.1

Table 3A .Numbers of $q\bar{q} \rightarrow b\bar{b}$ events (divided by 10^3) in Q^2 and x intervals at $L_{int} = 10 \text{ fb}^{-1}$.

Q^2 (GeV 2)	x values of a parton				All x 10^{-4}
	10^{-4}	10^{-3}	10^{-2}	10^{-1}	
1600-2500	143.6	508.5	578.3	104.8	1335.3
2500-5000	51.3	328.2	432.1	94.8	906.5
5000-10000	4.3	42.0	59.0	13.7	119.0
10000-20000	0	5.2	9.2	2.8	17.2
20000-40000	0	0.9	0.9	1.0	2.8
40000-80000	0	0.1	0.4	0.2	0.7

Table 4A .Numbers of $q\bar{q} \rightarrow g + g$ events (divided by 10^3) in Q^2 and x intervals at $L_{int} = 10 \text{ fb}^{-1}$.

Q^2 (GeV 2)	x values of a parton				All x 10^{-4}
	10^{-4}	10^{-3}	10^{-2}	10^{-1}	
1600-2500	89.3	473.6	489.1	50.5	1102.4
2500-5000	15.5	177.3	165.6	19.4	377.7
5000-10000	4.3	17.6	29.5	10.3	61.6
10000-20000	0	2.6	2.2	1.9	6.7
20000-40000	0	0.2	0.4	0.2	0.8
40000-80000	0	0	0.02	0.01	0.03

Table 5A . Numbers of $q\bar{q} \rightarrow q + \gamma$ events (divided by 10^3) in Q^2 and x intervals at $L_{int} = 10 \text{ fb}^{-1}$. m_{es} separation efficiencies are taken into account.

Q^2 (GeV=c) ²	x values of a parton				All x $10^4\{10^0$
	$10^4\{10^3$	$10^3\{10^2$	$10^2\{10^1$	$10^1\{10^0$	
1600-2500	945.0	2387.4	2608.6	246.7	6187.8
2500-5000	410.5	1723.1	1865.0	253.0	4251.7
5000-10000	41.3	443.2	475.5	134.6	1094.6
10000-20000	2.6	105.0	114.5	58.7	281.0
20000-40000	0	20.9	25.9	17.3	64.2
40000-80000	0	4.0	6.3	5.3	15.7

Table 6A . Numbers of $q\bar{q} \rightarrow q + g$ events (divided by 10^3) in Q^2 and x intervals at $L_{int} = 10 \text{ fb}^{-1}$. m_{es} separation efficiencies are taken into account.

Q^2 (GeV=c) ²	x values of a parton				All x $10^4\{10^0$
	$10^4\{10^3$	$10^3\{10^2$	$10^2\{10^1$	$10^1\{10^0$	
1600-2500	109.5	142.9	192.6	451.0	490.2
2500-5000	39.2	185.1	196.8	29.7	451.0
5000-10000	7.0	48.7	54.1	17.9	127.8
10000-20000	0.6	13.8	12.1	8.8	35.4
20000-40000	0	3.5	3.2	3.5	10.2
40000-80000	0	0.7	1.3	1.1	3.2

Table 7A . Numbers of γ brems events (divided by 10^3) in Q^2 and x intervals at $L_{int} = 10 \text{ fb}^{-1}$. m_{es} separation efficiencies are taken into account.

Q^2 (GeV=c) ²	x values of a parton				All x $10^4\{10^0$
	$10^4\{10^3$	$10^3\{10^2$	$10^2\{10^1$	$10^1\{10^0$	
1600-2500	129.9	394.3	476.6	87.2	1088.0
2500-5000	46.7	258.5	359.8	74.8	739.8
5000-10000	3.9	34.0	47.1	11.7	96.6
10000-20000	0	4.4	7.1	2.4	13.9
20000-40000	0	0.8	0.7	0.9	2.4
40000-80000	0	0.1	0.3	0.2	0.6

Table 8A . Numbers of m_{es} events (divided by 10^3) in Q^2 and x intervals at $L_{int} = 10 \text{ fb}^{-1}$. m_{es} separation efficiencies are taken into account.

Q^2 (GeV=c) ²	x values of a parton				All x $10^4\{10^0$
	$10^4\{10^3$	$10^3\{10^2$	$10^2\{10^1$	$10^1\{10^0$	
1600-2500	30.2	148.5	155.2	15.4	349.4
2500-5000	6.4	53.9	56.6	6.4	123.3
5000-10000	1.9	6.9	11.2	4.6	24.6
10000-20000	0	1.1	0.9	0.8	2.8
20000-40000	0	0.1	0.3	0.1	0.5
40000-80000	0	0	0.01	0.01	0.02

Table 9A. Numbers of $q\bar{q} + g$ events (divided by 10^3) in Q^2 and x intervals at $L_{int} = 10 \text{ fb}^{-1}$. m_{es} and $q=g$ separation efficiencies are taken into account.

Q^2 (GeV=c) ²	x values of a parton				All x $10^4 \{10^0$
	$10^4 \{10^3$	$10^3 \{10^2$	$10^2 \{10^1$	$10^1 \{10^0$	
1600-2500	623.7	1575.7	1721.7	162.8	4084.0
2500-5000	271.0	1137.3	1230.9	167.0	2806.2
5000-10000	27.3	292.5	313.8	88.9	722.5
10000-20000	1.7	69.4	75.6	38.7	185.5
20000-40000	0.0	13.8	17.1	11.5	42.4
40000-80000	0.0	2.7	4.2	3.5	10.4

Table 10A. Numbers of $q\bar{q} + g$ events (divided by 10^3) in Q^2 and x intervals at $L_{int} = 10 \text{ fb}^{-1}$. m_{es} and $q=g$ separation efficiencies are taken into account.

Q^2 (GeV=c) ²	x values of a parton				All x $10^4 \{10^0$
	$10^4 \{10^3$	$10^3 \{10^2$	$10^2 \{10^1$	$10^1 \{10^0$	
1600-2500	29.1	37.8	51.0	12.0	129.9
2500-5000	9.9	46.2	48.9	7.5	112.4
5000-10000	1.5	10.7	11.9	3.9	27.9
10000-20000	0.1	2.6	2.3	1.7	6.7
20000-40000	0.0	0.7	0.6	0.7	1.9
40000-80000	0.0	0.1	0.2	0.2	0.6

Table 11A. Numbers of $b\bar{b}$ events (divided by 10^3) in Q^2 and x intervals at $L_{int} = 10 \text{ fb}^{-1}$. m_{es} and $q=g$ separation efficiencies are taken into account.

Q^2 (GeV=c) ²	x values of a parton				All x $10^4 \{10^0$
	$10^4 \{10^3$	$10^3 \{10^2$	$10^2 \{10^1$	$10^1 \{10^0$	
1600-2500	48.5	147.1	177.8	32.5	406.0
2500-5000	17.2	95.0	132.2	27.5	272.0
5000-10000	1.4	12.2	17.0	4.2	34.8
10000-20000	0.0	1.6	2.6	0.9	5.1
20000-40000	0.0	0.3	0.3	0.3	0.9
40000-80000	0.0	0.0	0.1	0.1	0.2

Table 12A. Numbers of m_{es} events (divided by 10^3) in Q^2 and x intervals at $L_{int} = 10 \text{ fb}^{-1}$. m_{es} and $q=g$ separation efficiencies are taken into account.

Q^2 (GeV=c) ²	x values of a parton				All x $10^4 \{10^0$
	$10^4 \{10^3$	$10^3 \{10^2$	$10^2 \{10^1$	$10^1 \{10^0$	
1600-2500	19.9	98.0	102.5	10.2	230.6
2500-5000	4.2	35.6	37.4	4.2	81.4
5000-10000	1.3	4.6	7.4	3.0	16.2
10000-20000	0.0	0.8	0.6	0.5	1.9
20000-40000	0.0	0.1	0.2	0.1	0.3
40000-80000	0.0	0.0	0.01	0.01	0.02

